Solid-Fluid Transition in a Granular Shear Flow

Ashish V. Orpe and D.V. Khakhar*

Department of Chemical Engineering, Indian Institute of Technology-Bombay, Powai, Mumbai 400076, India

(Received 23 February 2004; published 2 August 2004)

The rheology of a granular shear flow is studied in a quasi-2D rotating cylinder. Measurements are carried out near the midpoint along the length of the surface flowing layer where the flow is steady and nonaccelerating. Streakline photography and image analysis are used to obtain particle velocities and positions. Different particle sizes and rotational speeds are considered. We find a sharp transition in the apparent viscosity (η) variation with rms velocity (u). Below the transition depth we find that the rms velocity decreases with depth and $\eta \propto u^{-1.5}$ for all the different cases studied. The material approaches an amorphous solidlike state deep in the layer. The velocity distribution is Maxwellian above the transition point and a Poisson velocity distribution is obtained deep in the layer. The results indicate a sharp transition from a fluid to a fluid + solid state with decreasing rms velocity.

DOI: 10.1103/PhysRevLett.93.068001 PACS numbers: 45.70.Mg, 83.80.Fg

Granular materials are known to exist in solidlike and fluidlike states [1]. Physical understanding of the flow of granular materials has thus developed along two major themes based on the flow regime [2]. In the *rapid flow* —fluidlike—regime, both theory and experimental analysis are generally cast in the framework of the kinetic theory [3]. In contrast, the *slow flow* —solidlike—regime is most commonly described using the tools of soil mechanics and plasticity theory [4] and recently by analogy to glasses [5–7]. These two approaches have no well-understood region of overlap. Given the qualitative differences between the fluid and solid states, a question that has been open for some time relates to the criterion for transition between fluid and solid states of granular materials. We focus on this question.

There are few studies which focus on the transition. Metcalfe *et al.* [8] studied solid to fluid transition in a horizontally vibrated container of beads. They observed hysteresis in the transition which was well predicted by a dry friction model in which the friction coefficient varies smoothly between a dynamic and a static value. A fluid-solid transition was also observed by D'Anna and Gremaud [5] for vertically vibrated particles. After a sharp transition to a supercooled liquid, the material gradually achieves a solidlike state on reducing the intensity of vibration following a modified Vogel-Fulcher-Tammann model typical of fragile glasses.

Coexisting solid and fluid phases have been studied primarily in the context of surface flows; these comprise a layer of fluidlike flow on a fixed bed of the same material. Examples of surface flows which have been well studied include heap flows [9–15] and rotating cylinder flows [16–22]. Remarkably simple theories describe the coexistence between the solid and the fluid. In the simplest versions, the local *melting* and *freezing* is determined by the local angle of the solid-fluid interface: If the local angle is greater than a "neutral" angle, the solid melts (the heap erodes) so as to reduce the angle and vice versa [9,10]. Continuum models based on Coulombic friction models for the solid region and simple rheological models for fluid region predict a similar behavior [12,15]. Experimental studies show that the models based on local angle based melting/freezing give good predictions [15].

An assumption in the coarse-grained models described above is the existence of an interface between the solid and the fluid. However, the recent work of Komatsu *et al.* [13] indicates that the surface flow on a heap decays smoothly with depth and generates motion deep within the heap. Studies of the velocity profile in rotating cylinder flow also confirm this picture of a smooth decay of the velocity into the bed, rather than an abrupt change at an interface [20,22].

The objective of the present work is to gain an insight into the fluid-solid transition in granular flows focusing on a system where both fluidlike and solidlike regions coexist. We find a well-defined transition point in the system which demarcates two distinct flow regions. The behavior in each region is characterized.

Experiments are carried out in quasi-2D aluminum cylinders (length 1 or 2 cm) of radius 16 cm [Fig. 1(a)]. The end walls are made of glass and a computer controlled stepper motor with a sufficiently small step is used to rotate the cylinders. Monodisperse, spherical, shiny stainless steel balls of three different sizes are used in the experiments (Table I). Cylinder rotation in the rolling flow regime (rotational speed, $\omega = 3$–9 rpm) produces a shallow flowing surface layer and measurements are made near the center of the cylinder where the layer thickness is maximum and the flow is nonaccelerating. The particles are heavy enough and conductive so that charge effects are negligible. The experiments are carried out with 50% of the cylinder filled with particles.

The motion of the particles is captured by taking high resolution images using a digital camera (Nikon Coolpix 5000). The size of the recorded region is 2560×1920 pixels, with one pixel corresponding to 0.016–0.03 mm

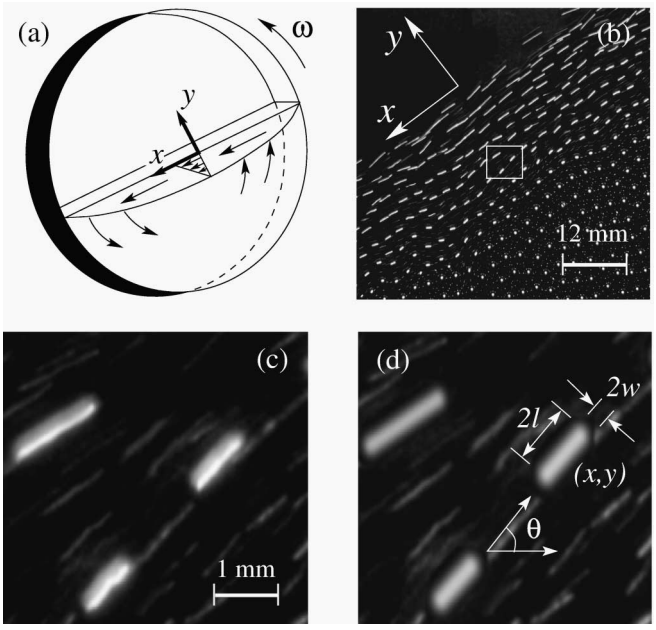

FIG. 1. (a) Schematic of the rotating cylinder geometry showing the flowing layer and the coordinate system employed. (b) A typical image showing the portion of the flowing layer at the center of the cylinder, with streaks of various lengths formed across the layer for a shutter speed of 1/250 s. (c) Magnified image of the rectangular region marked in (b) showing streaks generated by three different particles. (d) The same three streaks with the fitted intensity function. The optimization yields length ($2l$), width ($2w$), orientation angle (θ), and centroid position (x, y) for every streak.

depending on the distance of the camera to the cylinder. The point source of light is directed near parallel to the end wall of the cylinder so as to illuminate only the front layer of the flowing particles. Each moving particle generates a streak of definite length depending on its speed and the shutter speed of the camera. Images are taken for a range of camera shutter speeds (1/15–1/2000 s) so as to account for the varying velocity across the flowing layer. This gives streaks, which are adequately long for analysis but not so long as to overlap with other streaks, in each part of the flowing layer [Fig. 1(b)]. Two hundred images are taken for each shutter speed with an overall two thousand images combined over different shutter speeds. Because of the time interval between photographs, each experiment typically takes 500 cylinder revolutions (~ 3 h at 3 rpm).

A parametrized intensity function corresponding to a stretched Gaussian function is then fitted to the intensity values of the streak pixels (and an immediate neighborhood) in the image using Powell's method [23] for nonlinear optimization. The fitting yields the length ($2l$), width ($2w$), orientation angle (θ), and the centroid position (x, y) for the streak [Fig. 1(d)]. The analysis technique was calibrated by carrying out experiments with a single particle glued to the inside of the cylinder face plate. The error in velocity measurements was found to be less than 3%. The flowing layer region is divided into bins of width equal to the particle diameter and length 20 mm parallel to the flowing layer, and the components of the mean and the root mean square (rms) velocities for each bin are calculated by averaging over all streaks in a bin.

TABLE I. Mass (m) and diameter (d) of the particles used in the experiments.

d (mm)	1	2	3
m (mg)	4.2 ± 0.06	33.5 ± 0.18	112.5 ± 0.18

Figure 2 gives the variation of the mean velocity, the rms velocity, number density, shear rate, and shear stress with depth (y) in the flowing layer for 2 mm particles. The error bars show the standard deviation over ten data sets. The mean velocity ($\langle v_x \rangle$) profile is smooth and shows three regions: a near-linear middle region, an exponentially decaying region at the bottom, and a flattened region near the top. Similar profiles have been reported in several previous studies [20–22,24–29]. The flattened upper region corresponding to the low density region of saltating particles is not seen in some studies [22,29]. The profile of the rms velocities (u) is shown in Fig. 2(b). The rms velocity profile shows two distinct regions: a relatively slow variation near the free surface followed by a sharper decrease deeper in the bed. A low value is obtained at the free surface ($y = 0$) because particle trajectories are ballistic in that region due to the very low number densities [Fig. 2(c)] and high velocities [Fig. 2(a)]. The areal number density (n) is almost constant throughout the flowing layer with a rapid decrease near the free surface [Fig. 2(c)]. Figure 2(d) shows the shear rate ($\dot{\gamma}$) variation in the layer, obtained by numerical differentiation of the data in Fig. 2(a). The shear rate increases to a maximum value (corresponding to the inflection point in the velocity field) and then decreases. We note that an oscillating shear rate profile is obtained if a smaller bin size is used as reported previously [21,26,28]. The transition point in the rms velocity profile coincides with the maximum in the shear rate.

For nonaccelerating flows, a force balance yields the shear stress as $d\tau_{yx}/dy = \rho g \sin\beta \approx \rho_b (n/n_b) g \sin\beta$, where g is acceleration due to gravity, β is the inclination of the flowing layer, n_b is the number density in the rotating packed bed, and ρ_b is the bulk density of the rotating packed bed. We neglect the contribution of wall friction in the estimate. This could become significant deeper in the bed [27]. However, based on the method of Taberlet *et al.* [27], we find that the contribution is about 10% of the total stress in the cases studied and does not qualitatively affect the results. Upon integration, we obtain $\tau_{yx} = (\rho_b/n_b) g \sin\beta \int_y^0 n dy$ assuming $\tau_{xy} = 0$ at the free surface. The shear stress shows a near linear increase with depth [Fig. 2(e)]. The results of Figs. 2(d) and 2(e) indicate that there is a qualitative change in the rheology

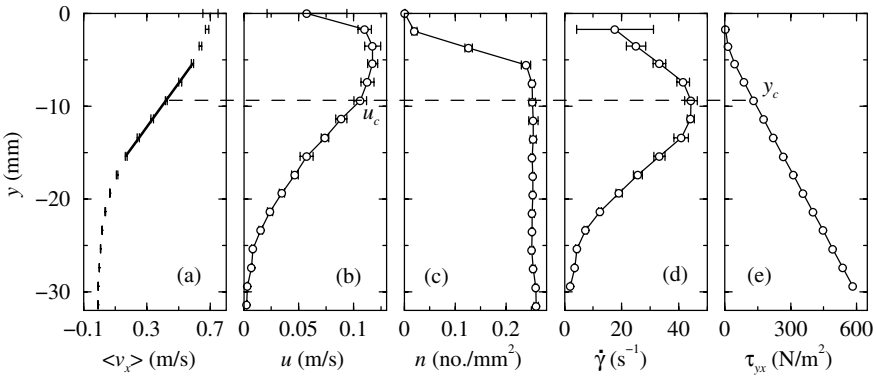

FIG. 2. Mean velocity ($\langle v_x \rangle$), rms velocity (u), number density (n), shear rate ($\dot{\gamma}$), and shear stress (τ_{yx}) across the flowing layer for 2 mm steel balls rotated at 3 rpm. The error bars indicate the standard deviation over ten data sets. The solid line in (a) is a linear fit to the mean velocity profile and the dashed line denotes the depth of transition point (y_c).

at the transition point (y_c). Above y_c, the shear stress increases with shear rate which is typical of fluids. However, below y_c the shear stress increases while the shear rate decreases. This implies that the viscosity increases sharply with depth below y_c, even though the number density is nearly constant [see inset of Fig. 3(a)].

Figure 3(a) shows the variation of the apparent viscosity ($\eta = \tau_{yx}/\dot{\gamma}$) with the rms velocity (u). The data points at and above the transition point ($y \geq y_c$) are plotted as filled symbols. There is a sharp transition in this case as well and the transition occurs at the same value of u as in Fig. 2(b). In the region near the free surface, there is a rapid increase in viscosity with decreasing rms velocity whereas in the region approaching the fixed bed there is a much slower power law increase with an exponent -1.5 for all the cases studied. The data below the transition point ($y \leq y_c$) scales with the particle mass m, the average shear rate ($\dot{\gamma}_{\text{avg}}$), and d to fall on a single curve [Fig. 3(b)], and the transition occurs at $u_c \sim 1.2\dot{\gamma}_{\text{avg}} d$ for all cases. Here $\dot{\gamma}_{\text{avg}}$ is the shear rate obtained by fitting a straight line to the linear portion of the velocity profile [Fig. 2(a)]. Although the choice of range for the fit may appear somewhat arbitrary, the average shear rate obtained varies less than 5% when the number of points used in the fit are varied. The typical variation of viscosity with depth is shown for one case in Fig. 3(a) (inset). The viscosity diverges with depth in the layer consistent with the above results.

Figure 4 shows the distributions of the y-direction velocity at different locations (y) across the flowing layer. The v_y distribution is Gaussian for all points above the transition point [$y \geq y_c$, Fig. 4(a)] and it gradually evolves to a Poisson distribution as we go deeper into the bed [Fig. 4(b)]. The v_x distribution (not shown) is Gaussian above the transition point. However, below the transition point the behavior is complex and bimodal distributions are obtained. The Maxwellian distribution of velocities above the transition point implies fluidlike behavior. The gradual transition to a Poisson velocity distribution with depth indicates an increasing fraction of solidlike material. A similar approach to a Poisson velocity distribution with depth was found by Mueth [26] for dense Couette flow.

The results presented show a sharp transition between two distinct flow regimes. In the upper region near the free surface, the behavior is fluidlike and the velocity

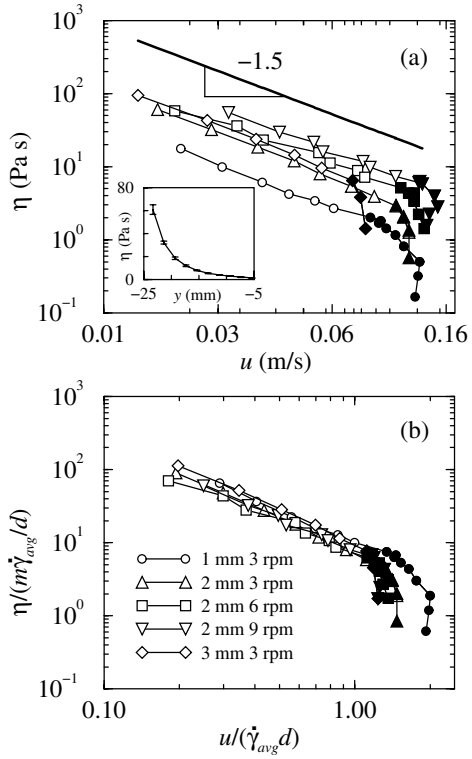

FIG. 3. Apparent viscosity (η) variation with rms velocity (u) for all the cases studied. Filled symbols represent the points at and above the transition velocity (u_c). (a) The solid line at the top represents a linear fit (slope $\simeq -1.5$) to the data below the transition point for all the cases studied. Inset: Variation of η across the flowing layer depth (y) for 2 mm steel balls rotated at 3 rpm. (b) The data is scaled using particle mass (m), particle diameter (d), and average shear rate ($\dot{\gamma}_{\text{avg}}$) obtained by a linear fit to each corresponding velocity profile.

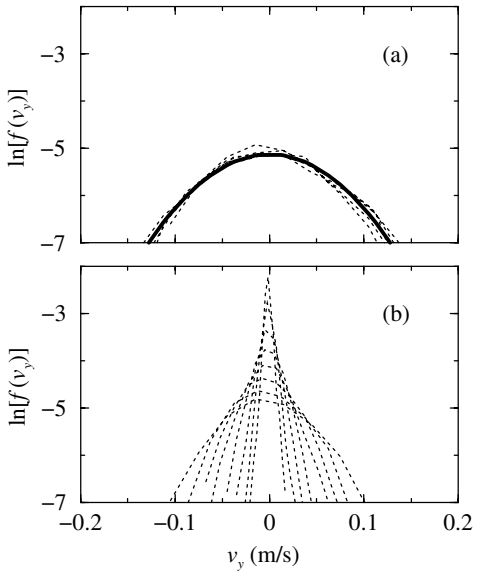

FIG. 4. Distributions of velocity in the y direction at various locations across the layer for 2 mm steel balls rotated at 3 rpm. (a) The fluidlike region at and above the transition point; the solid line represents a fitted Maxwellian distribution to the curves at and above the transition point. (b) The region below the transition point.

distributions are Maxwellian. Below the transition point, the material appears to be an amorphous soft solid, increasing in strength with depth in the layer. The transition to this solidlike regime occurs at a relatively large rms velocity (0.05–0.1 m/s) and in a region of constant number density (n). We conjecture that the sharp transition occurs because of the formation of a percolated network of particles in extended contact with each other. This is in contrast to the fluidlike regime where the particles interact through collisions. The contact network coexists with fluidlike domains and the fraction of particles which are part of the network increase with depth. This picture for the region below the transition point is broadly consistent with recent measurements of Bonamy *et al.* [30] in which flowing clusters were identified, as well as with nonlocal models based on the coexistence of particle chains and fluidlike material [31,32]. However, a more detailed study is needed to verify this and to understand the nature of the transition.

The financial support of Department of Science and Technology, India, through the Swarnajayanti Fellowship project (DST/SF/8/98) is gratefully acknowledged.

*Electronic address: khakhar@iitb.ac.in

[1] H. M. Jaeger, S. R. Nagel, and R. P. Behringer, Rev. Mod. Phys. **68**, 1259 (1996).
[2] R. Jackson, J. Rheol. (N.Y.) **30**, 907 (1986).
[3] C. S. Campbell, Annu. Rev. Fluid Mech. **22**, 57 (1990).
[4] R. M. Nedderman, *Statics and Kinematics of Granular Materials* (Cambridge University Press, Cambridge, England, 1992).
[5] G. D'Anna and G. Gremaud, Nature (London) **413**, 407 (2001).
[6] A. Barrat, J. Kurchan, V. Loreto, and M. Sellitto, Phys. Rev. E **63**, 051301 (2001).
[7] J. Kurchan, J. Phys. Condens. Matter **12**, 6611 (2000).
[8] G. Metcalfe, S. G. K. Tennakoon, L. Kondic, D. G. Schaeffer, and R. P. Behringer, Phys. Rev. E **65**, 031302 (2002).
[9] J. P. Bouchaud, M. E. Cates, J. Ravi Prakash, and S. F. Edwards, J. Phys. I (Paris) **4**, 1383 (1994).
[10] T. Boutreux, E. Raphaël, and P. G. de Gennes, Phys. Rev. E **58**, 4692 (1998).
[11] Y. Grasselli and H. J. Herrmann, Eur. Phys. J. B **10**, 673 (1999).
[12] S. Douady, B. Andreotti, and A. Daerr, Eur. Phys. J. B **11**, 131 (1999).
[13] T. S. Komatsu, S. Inagaki, N. Nakagawa, and S. Nasuno, Phys. Rev. Lett. **86**, 1757 (2001).
[14] P.-A. Lemieux and D. J. Durian, Phys. Rev. Lett. **85**, 4273 (2000).
[15] D. V. Khakhar, A. V. Orpe, P. Andresén, and J. M. Ottino, J. Fluid Mech. **441**, 255 (2001).
[16] J. Rajchenbach, Phys. Rev. Lett. **65**, 2221 (1990).
[17] T. Elperin and A. Vikhansky, Europhys. Lett. **42**, 619 (1998).
[18] A. V. Orpe and D. V. Khakhar, Phys. Rev. E **64**, 031302 (2001).
[19] D. V. Khakhar, A. V. Orpe, and J. M. Ottino, Adv. Complex Systems **4**, 407 (2001).
[20] N. Jain, J. M. Ottino, and R. M. Lueptow, Phys. Fluids **14**, 572 (2002).
[21] K. M. Hill, G. Gioia, and V. V. Tota, Phys. Rev. Lett. **91**, 064302 (2003).
[22] D. Bonamy, F. Daviaud, and L. Laurent, Phys. Fluids **14**, 1666 (2002).
[23] W. H. Press, S. A. Teukolsky, W. T. Vellerling, and B. P. Flannery, *Numerical Recipes in Fortran: The Art of Scientific Computing* (Cambridge University Press, Cambridge, England, 1994), Chap. 10, 2nd ed.
[24] L. Bocquet, W. Losert, D. Schalk, T. C. Lubensky, and J. P. Gollub, Phys. Rev. E **65**, 011307 (2001).
[25] S. Longo and A. Lamberti, Exp. Fluids **32**, 313 (2002).
[26] D. M. Mueth, Phys. Rev. E **67**, 011304 (2003).
[27] N. Taberlet, P. Richard, A. Valance, W. Losert, J. M. Pasini J. T. Jenkins, and R. Delannay, Phys. Rev. Lett. **91**, 264301 (2003).
[28] D. M. Mueth, G. F. Debregeas, G. S. Karczmar, P. J. Eng, S. R. Nagel, and H. M. Jaeger, Nature (London) **406**, 385 (2000).
[29] J. Rajchenbach, E. Clement, and J. Duran, in *Fractal Aspects of Materials*, edited by F. Family *et al.* (MRS Symposium, Pittsburgh, 1995), Vol. 367, pp. 525–528.
[30] D. Bonamy, F. Daviaud, L. Laurent, M. Bonetti, and J. P. Bouchaud, Phys. Rev. Lett. **89**, 034301 (2002).
[31] P. Mills, D. Loggia, and M. Tixier, Europhys. Lett. **45**, 733 (1999).
[32] D. Bonamy and D. Mills, Europhys. Lett. **63**, 42 (2003).